Towards Anti-interference WiFi-based Activity Recognition System Using Interference-Independent Phase Component

Jinyang Huang*, Bin Liu*, Pengfei Liu*, Chao Chen†, Ning Xiao*, Yu Wu*, Chi Zhang*, Nenghai Yu*
*CAS Key Laboratory of Electromagnetic Space Information, University of Science and Technology of China, Hefei, China
†Institute of Information Science and Electronic Engineering, Zhejiang University, Hangzhou, China
{huangjy, liupf17, xiaoning, wy}@mail.ustc.edu.cn, {flowice,chizhang,ynh}@ustc.edu.cn, chench@zju.edu.cn

***Abstract*—Human activity recognition (HAR) has become increasingly essential due to its potential to support a broad array of applications, e.g., elder care, and VR games. Recently, some pioneer WiFi-based HAR systems have been proposed due to its privacy-friendly and device-free characteristics. However, their crucial limitation lies in ignoring the inevitable impact of co-channel interference (CCI), which degrades the performance of these HAR systems significantly. To address this challenge, we propose PhaseAnti, a novel HAR system to exploit the CCI-independent phase component, NLPEV (Nonlinear Phase Error Variation), of Channel State Information (CSI) to cope with the impact of CCI. We provide a rigorous analysis of NLPEV data with respect to its stability and otherness. Validated by our experiments, this phase component across subcarriers is invariant to various CCI scenarios, while different for distinct motions. Based on the analysis, we use NLPEV data to perform HAR in CCI scenarios. Extensive experiments demonstrate that PhaseAnti can reliably recognize activity in various CCI scenarios. Specifically, PhaseAnti achieves a 95% recognition accuracy rate (RAR) on average, which improves up to 16% RAR in the presence of CCI. Moreover, the recognition speed is $9\times$ faster than the state-of-the-art solution.**

I. Introduction

A. Backgrounds and Motivations

Human activity recognition (HAR) is the core technology that enables novel applications in different areas, such as health care, entertainment, and security [1]. Traditional approaches use cameras [2], [3] and wearable sensors [4], [5] to perform HAR. However, camera-based approaches have the fundamental limitations of requiring enough light, and the privacy leak problem cannot be ignored. Wearable sensor-based methods are inconvenient sometimes since the sensors have to be worn on the users' body. Recently, WiFi-based HAR systems [6]–[11] have been proposed. WiFall [7] exploited the unique diversity of Channel State Information (CSI) to detect human fall in the indoor environment. QGesture [11] used CSI values to measure the movement distance and direction of human hands. Their crucial advantages over camera-based and sensor-based methods are that they do not need lighting, preserve user privacy, operate through walls, and do not require users to carry any devices as they rely on the signals reflected by the human body.

However, the key limitation of these WiFi-based HAR systems is that they ignore the effects of co-channel interference (CCI), which leads to a sharp drop in the performance under CCI scenarios. Unfortunately, CCI becomes more common since the number and types of WiFi devices have proliferated in the last decade and often varies due to channel hopping mechanism [12]. Thus, it is almost impossible to find a channel that is clean or only occupied by one node within the signal coverage. For instance, Fig. 1 shows that the mobile phone receives multiple router signals in one place, but the spectrum of some router channels is overlapped with the connection channel. Thus, the CCI happens. Moreover, CCI has severe negative impacts on WiFi signals, i.e., the confusion of signal amplitude [13], [14], and the subcarrier correlation weakens [15], which finally results in the degradation of HAR system performance. Therefore, an anti-interference HAR system to recognize motions accurately in CCI scenarios is necessary and valuable.

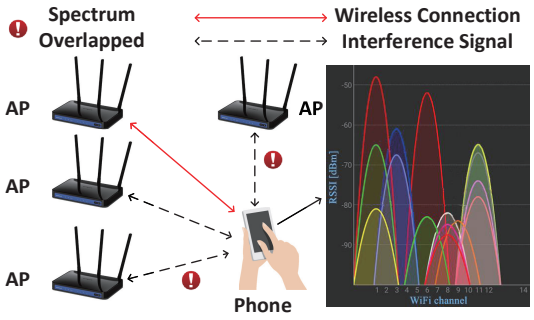

Fig. 1 Indoor environment of electromagnetic.

B. Challenges and Contributions

Indeed, for an anti-interference HAR system, the signal component used for recognition should be invariant across different CCI scenarios and time, but sensitive and distinct for different motions. If the signal component itself changes with CCI, it is difficult to extract the only motion-related part from this signal component. However, the CSI amplitude used by most WiFi-based HAR systems [6]–[10] is varying in CCI scenarios since different nodes within the signal coverage adjust its sending power to better compete for the channel [15]. Thus, CSI amplitudes do not satisfy the requirement of the anti-CCI signal component. Fortunately, CSI phases are not affected by the varying transmission power caused by CCI. Therefore, the CCI-independence component can be extracted from the CSI phase. Besides,

to satisfy the universal property, the anti-interference HAR system should be deployable on existing infrastructure. Furthermore, the low time delay is also an essential requirement for HAR systems, and it is inappropriate to spend too much signal processing time to reduce the impact of CCI.

Thus, three challenges need to be formally addressed before realizing a novel anti-CCI CSI-based HAR system.

- **Stable signal component *vs.* Varying CSIs:** The CSI amplitude used by most pioneer HAR systems is varying with the CCI change. Besides, due to the significant variations caused by noises, and the unsynchronized time and frequency at transmitter and receiver, the CSI phase initially contains many errors [11], and these phase errors are difficult to eliminate. Therefore, it is challenging to extract the CCI robustness and only motion-related signal component from varying CSIs.
- **Universal equipment *vs.* Complex function:** The specialized radio frequency equipment can select a unique channel to avoid CCI, and the impact of CCI can also be degraded by increasing the sending power. However, these methods are expensive to implement in daily life or have side effects on other wireless signals, e.g., Bluetooth and Zigbee. Thus, How to realize the complex function of anti-interference with universal equipment becomes a question worthy of consideration.
- **Fast recognition speed *vs.* High computational complexity:** In order to achieve a fast recognition speed, the computational complexity needs to reduce. However, most existing subcarrier fusion algorithms for data dimension reduction become ineffective since the weak subcarrier correlation caused by CCI [15]. Thus, how to select subcarriers in CCI scenarios to balance accuracy and speed becomes an inevitable problem.

To tackle these challenges, we propose PhaseAnti, an anti-CCI HAR system based on WiFi CSI. Specifically, by eliminating irrelevant errors, the phase component NLPEV is leveraged from the off-the-shelf WiFi device since this component keeps constant for CCI and contains motion information. Then, a suitable calibration method is introduced to make NLPEV data stable and sensitive to motions. Next, to reduce the data dimension, a novel subcarrier selection algorithm is used with less information loss. Finally, by using this calibrated data of the selected subcarrier to perform HAR in CCI scenarios, the activity can be recognized accurately with low recognition time.

In total, we make the following contributions:

- We propose a novel Anti-interference, Non-intrusive HAR system PhaseAnti leveraging CSI from a single commodity WiFi device.
- As far as we know, this work is the first to present a CCI-independence component of CSI and the first to use the CSI phase component to perform HAR in CCI scenarios. We carefully verify the invariance of the proposed component NLPEV to various CCI scenarios and the difference of this component to distinct activities.
- Instead of fusing subcarrier simply, we design an effective algorithm to choose subcarriers according to the sensitivity of the subcarrier to movements. We show that this algorithm can select subcarriers with more motion information while reducing the data dimension.
- Extensive experiments with different motions have been performed in various CCI scenarios. The results show that PhaseAnti improves up to 16% recognition accuracy rate on average in the presence of complex CCI, reaching 95%, and the recognition speed is $9\times$ faster than the pioneer anti-CCI HAR solution [15].

The rest of the paper is organized as follows. We first present the preliminaries of CSI and the analysis of NLPEV data in Section II. We then describe the PhaseAnti design in Section III. Implementation and evaluation are presented in Section IV. Section V discusses the related works. Finally, we conclude our work in Section VI.

II. Preliminaries And NLPEV Analysis

A. Channel State Information Preliminaries

Network Interface Cards (NICs) continuously capture variations in the wireless channel using CSI, which is fine-grained physical layer information and characterizes the channel frequency response (CFR) of the wireless channel [12]. CSI reveals the channel characteristics experienced by the received signals, such as the effect of scattering, multipath effect, and power decay [16]. Since WiFi systems commonly use Orthogonal Frequency Division Multiplexing (OFDM) technology, the channel between each transmitter-receiver (Tx-Rx) antenna pair consists of multiple subcarriers [8]. Let $\boldsymbol{X}_i$ and $\boldsymbol{Y}_i$ be the frequency domain representations of the transmitted and the received signals of i^{th} transmitter-receiver pair, respectively. Thus, the two signals can be related by the expression:

$$\boldsymbol{Y}_i = \boldsymbol{H}_i \boldsymbol{X}_i + \boldsymbol{N}_i \tag{1}$$

where $\boldsymbol{H}_i$ is the complex-valued CFR of i^{th} Tx-Rx pair which can be estimated by transmitting a known preamble of OFDM symbols between the transmitter and the receiver [8], and $\boldsymbol{N}_i$ is the additive white Gaussian noise [9]. CSI measurements contain these CFR values, and the CFR of k^{th} subcarrier in i^{th} Tx-Rx pair can be expressed as:

$$\boldsymbol{H}_i{}^{(k)} = \left|\boldsymbol{h}_i{}^{(k)}\right| \cdot e^{-j\cdot\angle \boldsymbol{h}_i{}^{(k)}} = I_i{}^{(k)} + jQ_i{}^{(k)} \quad k \in \boldsymbol{K} \tag{2}$$

where $\left|\boldsymbol{h}_i{}^{(k)}\right|$ and $\angle \boldsymbol{h}_i{}^{(k)}$ denote the amplitude and the phase of k^{th} subcarrier in i^{th} Tx-Rx pair. Besides, the raw CFR estimated in NICs can also be recorded as the I/Q signal. I and Q are the in-phase component and the quadrature component, respectively. $\boldsymbol{K}$ contains the subcarrier indexes. Although the WiFi system has 56 subcarriers over a 20 MHz channel, the Intel 5300 NIC we use can only report CSI for 30 of the 56 subcarriers [17]. Specifically, for the Intel 5300 NIC, $\boldsymbol{K} = [-28, -26, \cdots, -2, -1, 1, 3, \cdots, 27, 28]$. The phase $\angle \boldsymbol{h}_i{}^{(k)}$ can be calculated from the I/Q component:

$$\boldsymbol{\phi} = \arctan(\frac{Q}{I}) \tag{3}$$

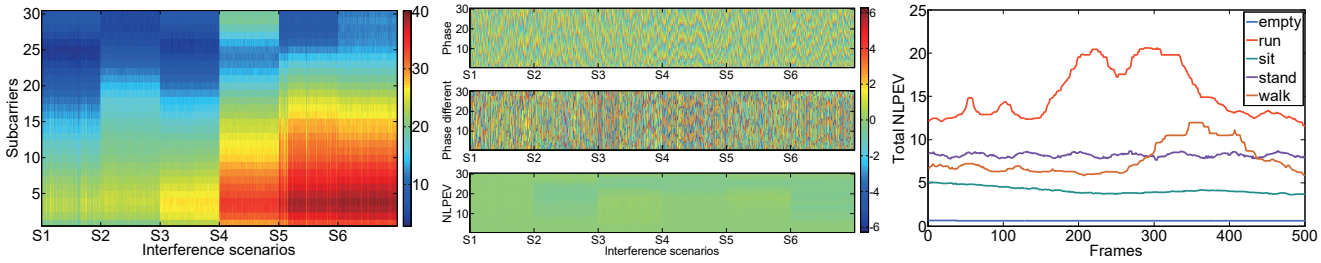

(a) CSI amplitude changes with various CCI scenarios. Red means a high subcarrier power.

(b) The impact of various CCI scenarios on different phase components.

(c) Total NLPEV of different activities. Frame: the received packet.

Fig. 2 Observation of the properties of different CSI signal components. Each CCI scenario contains 500 consecutive CSI frames, and the sampling rate is 100 Hz. All these CCI scenarios do not include human movements.

B. NLPEV

Due to the variant signal transmission environment and the imperfect hardware design, the measured phases at the receiver are different from the phases at the transmitter. Generally, the phase difference between transmitter and receiver can be grouped into two categories, i.e., linear phase errors (LPE) and nonlinear phase errors (NLPE) [18]. Especially, LPE and NLPE mean that the phase errors vary linearly or nonlinearly with subcarrier indexes, respectively.

According to [11], [19], [20], for a particular pair of transmitter and receiver, the phases of subcarriers measured at the receiver ϕ can be expressed as:

$$\phi = \varphi_I + \omega + \theta + \sigma + \gamma + \chi \tag{4}$$

where φ_I represents the real phases at the transmitter. ω, θ, σ, and γ denote the phase offsets due to packet boundary detection (PBD), sampling frequency offset (SFO), carrier frequency offset (CFO), and time of flight (ToF) respectively, and these phases are LPEs [20]. According to [18], imperfect hardware design causes an NLPE. Besides, by affecting multipath, the motion also causes an NLPE [21]. Thus, the last element χ can be written as:

$$\chi = \psi + \eta \tag{5}$$

where ψ and η are the NLPEs caused by imperfect hardware design and human motion, respectively. Since ψ is proved to be a constant for each specific network card [18], the change of χ equals to the variation of η caused by human movement. Therefore, by comparing the χ_m in the movement with the χ_{wm} in an empty room without human motion, the NLPE η caused by human movement can be estimated as:

$$\begin{aligned} \chi_m - \chi_{wm} &= \psi + \eta - (\psi + \eta_{em}) \\ \eta &= \chi_m - \chi_{wm} \end{aligned} \tag{6}$$

where η_{em} is the variation of NLPE without human movement and equals to 0 [18]. Thus, η can be estimated by nonlinear phase error variation (NLPEV) when NICs do no change. Section III-A shows the derivation process of η.

C. Preliminary Tests and Observations

We perform preliminary experiments to evaluate the stability of NLPEV for various CCI scenarios, and the difference of NLPEV for distinct activities. The specific settings of these CCI scenarios are shown in Tab. I.

TABLE I Setting for CCI scenarios. IAP: Interference AP. ITR: Interference traffic rate. Channel: IAP channel. The recognition AP is set to channel 1 in the 2.4 GHz band.

CCI scenarios	IAP number	ITR for each IAP	Channel
S1	0	None	None
S2	1	1 MB/s	2
S3	2	1 MB/s	2
S4	3	1 MB/s	2
S5	1	10 MB/s	2
S6	2	10 MB/s	2

As shown in Fig. 2(a), with the increasing of setting ITR, the amplitude of CSI subcarriers also rises. This is because the router increases its own power in more severe CCI to better compete for the channel. Thus, it is difficult to obtain a CCI-independence component from CSI amplitude. Fig. 2(b) depicts the impact of various CCI scenarios on different CSI phase components. Since many phase errors are included, the original phases are unstable and randomly change from $-\pi$ to π even when the CCI does not change. Besides, since the more general 2.4 GHz band exists much CCI, the stability of the phase difference data [9] generated by the subtraction of two receiver antenna phases and proved to be stable and effective in 5 GHz band, is affected. However, since all the phase errors are removed, and only the motion-related component is retained, the proposed phase component NLPEV keeps stable in various CCI scenarios and stays around 0 (η_{em}) since there is no motion. Fig. 2(c) depicts that different activities contribute differently to the output of total NLPEV time curves. Notably, the total NLPEV represents the sum of absolute values of 30 subcarrier NLPEVs. As shown in Fig. 2(c), the intense-motion, e.g., walking and running, make large NLPEV vibrations. However, the slow-motion, e.g., sitting, makes a small NLPEV fluctuation. Moreover, the total NLPEV keeps constant and approximately equals 0 when there is no motion.

These observations conclude that the amplitude-based methods are hardly able to realize anti-interference due to the unstable subcarrier amplitudes caused by varying CCI, which can seriously degrade the classification performance. Besides, other phase components like the original phase and the phase difference do not contain enough motion information due to lots of phase errors and CCI, respectively. However, the proposed CSI phase component NLPEV remains invariant across various CCI and time. Moreover, the

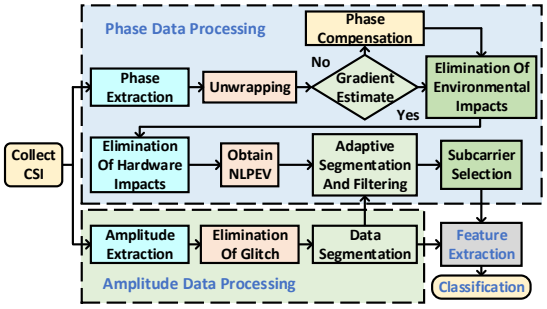

Fig. 3 Framework of PhaseAnti.

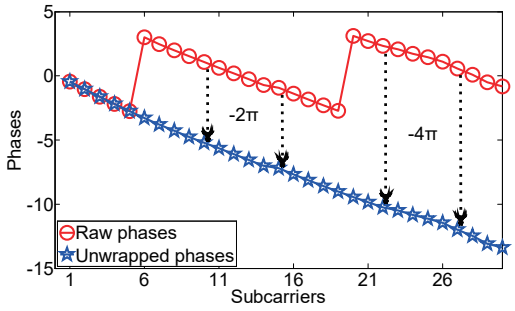

Fig. 4 Phase unwrapping.

NLPEVs caused by different human motions are distinct. Therefore, by extracting NLPEV data from the CSI phase to perform HAR, the system can achieve anti-interference.

III. PhaseAnti System Design

To achieve HAR in CCI scenarios, we design PhaseAnti, and its framework is shown in Fig. 3. The proposed system has two most crucial components, i.e., phase data processing unit, and amplitude data processing unit. Firstly, phase error elimination and NLPEV extraction are performed during the phase data processing. The crucial distinction of this component is that it is invariant across various CCI scenarios and time but different for distinct motions. Then, an amplitude data processing method is introduced to perform data segmentation of CSI amplitudes and use the segmentation information to realize the adaptive NLPEV data filtering and segmentation. Next, a subcarrier selection algorithm is proposed to reduce the data dimension. Finally, the features are extracted, and the activities are classified.

A. Phase and Amplitude Data Processing

Phase Extraction and Unwrapping: As introduced in Section II, the raw phases at the receiver can be measured according to Eq. (3). However, as shown in Fig. 4, the raw phases distribute between $-\pi$ and π due to the periodicity of the tangent function, which results in the ambiguity of the subcarrier relationship. Thus, to recover the real phases of all subcarriers, the raw phases are unwrapped by tracking the corresponding periodic integers of subcarriers [18]. With such unwrapping, the unwrapped phases of each subcarrier become an approximately linear curve.

Gradient Estimate and Phase Compensation: Due to the low RSSI of received signals and the unstable CSITOOL [17], not all of the subcarrier phases are measured accurately and unwrapped successfully [18], [20]. Moreover, these incorrectly measured phases are harmful to HAR due to phase aliasing. Thus, it is necessary to eliminate and then smooth the incorrectly measured phases of the sampled CSI frames. Fig. 5(a) depicts that some incorrectly unwrapped phases (marked with black triangles) change from one subcarrier to another subcarrier randomly with different gradients. As shown in Fig. 5(b), we observe that the gradients of regularly changing phases are more concentrated than the gradients of randomly changing phases (marked with red circles). Moreover, the gradient variances of randomly changing

algorithm 1 Phase filter based on gradient variances

Input: subcarrier phases of frames $\boldsymbol{U} = \{\boldsymbol{\phi}^1, \boldsymbol{\phi}^2, ...\}$.
Output: randomly changing phase frame indexes $\boldsymbol{Index}$.

```
for i := 1; i <= length(U); i++ do
    G^i := gradient(φ^i). //Gradient of phases.
    R^i := gradient(G^i).
    var := 0. //Variation of gradient.
    for k := 1; k <= 30; k++ do
        var := var + abs(R^i_k).
    end for
    if var/(30 × (max(R^i) − min(R^i))) > ν_max then
        Index.add(i).
    end if
end for
return Index.
```

phases are steep and prominent in all frames (marked with black rectangles). To find the frames with incorrectly measured phases, inspired by the above observation, we design an algorithm based on the gradient variance threshold to seek out the frames with larger phase gradient variance. Algorithm 1 describes the searching process.

From the cumulative distribution of the normalized gradient variances shown in Fig. 5(c), we can observe that the frames with randomly changing phases (larger variance) are few in all frames. Furthermore, Fig. 5(b) shows that these frames appear discontinuously. Thus, the frames with randomly changing phases can be smoothed and compensated to capture motions continuously. Specifically, the *moving average filtering* [22] with time weight is used to smooth the randomly changing phase frames. The smoothed phases of the frames in the $\boldsymbol{Index}$ can be expressed:

$$\boldsymbol{\phi}' = \frac{1}{W_{nor}} \sum_{i \in Nor} \boldsymbol{\phi}^i \quad Nor \subseteq W \tag{7}$$

$$W = S \cdot t_{act} \tag{8}$$

where $\boldsymbol{\phi}'$ is the smoothed phase, and W is the window size of the moving average filter, which is determined by the sampling rate S and the motion-related time factor t_{act}. To minimize the deviation caused by smoothing, based on empirical knowledge, t_{act} is set to 0.3s. Nor is the set of correctly unwrapped frames in W, and W_{nor} is the number of the correctly unwrapped frames in W.

Elimination of environmental impacts: As introduced in Section II, the subcarrier phases $\boldsymbol{\phi}$ measured at the receiver

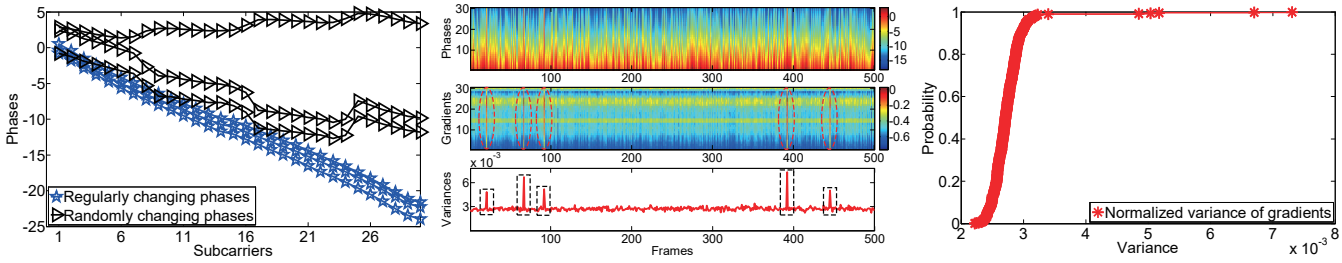

(a) Unwrapped phases of different frames. **(b)** Unwrapped phases, gradients, and normalized gradient variances. **(c)** CDF of normalized gradient variances.

Fig. 5 Unwrapped phase observation and filtering.

can be expressed as:

$$\boldsymbol{\phi} = \boldsymbol{\varphi_I} + \boldsymbol{\omega} + \boldsymbol{\theta} + \boldsymbol{\sigma} + \boldsymbol{\gamma} + \boldsymbol{\chi} \tag{9}$$

Specifically, the phase errors of PBD ($\boldsymbol{\omega}$) and SFO ($\boldsymbol{\theta}$) in the same frame are related to subcarrier index $\boldsymbol{K}$, which can be represented as:

$$\boldsymbol{\omega} = 2\pi\alpha \cdot \boldsymbol{K} \tag{10}$$

$$\boldsymbol{\theta} = 2\pi\beta \cdot \boldsymbol{K} \tag{11}$$

where α and β are constant depending on PBD and SFO. The offset of ToF $\boldsymbol{\gamma}$ is also related to subcarrier frequency:

$$\boldsymbol{\gamma} = 2\pi t_f \boldsymbol{F} \tag{12}$$

where t_f is ToF and affected by location. $\boldsymbol{F}$ is the set of subcarrier frequencies represented by the center frequency f_c, identity matrix $\vec{\boldsymbol{q}}$, the frequency difference between two adjacent subcarriers f_b (equals to 312.5 kHz [12]), and subcarrier index $\boldsymbol{K}$, i.e., $\boldsymbol{F} = f_c \cdot \vec{\boldsymbol{q}} + f_b \boldsymbol{K}$. Thus, the phase error caused by ToF $\boldsymbol{\gamma}$ can be rewritten as:

$$\begin{aligned} \boldsymbol{\gamma} &= 2\pi t_f \boldsymbol{F} \\ &= 2\pi t_f (f_c \cdot \vec{\boldsymbol{q}} + f_b \boldsymbol{K}) \\ &= 2\pi t_f f_c \cdot \vec{\boldsymbol{q}} + 2\pi t_f f_b \boldsymbol{K} \\ &= \boldsymbol{Z} + 2\pi t_f f_b \boldsymbol{K} \end{aligned} \tag{13}$$

where $2\pi t_f f_c \cdot \vec{\boldsymbol{q}}$ is independent of $\boldsymbol{K}$. In one frame, t_f is a constant value, so we use $\boldsymbol{Z}$ to replace the first part. In this respect, the phase measured at the receiver can be reformulated as:

$$\begin{aligned} \boldsymbol{\phi} &= \boldsymbol{\varphi_I} + \boldsymbol{\omega} + \boldsymbol{\theta} + \boldsymbol{\sigma} + \boldsymbol{\gamma} + \boldsymbol{\chi} \\ &= \boldsymbol{\varphi_I} + 2\pi\alpha \cdot \boldsymbol{K} + 2\pi\beta \cdot \boldsymbol{K} + \boldsymbol{\sigma} + \boldsymbol{Z} + 2\pi t_f f_b \cdot \boldsymbol{K} + \boldsymbol{\chi} \\ &= \boldsymbol{\varphi_I} + 2\pi(\alpha + \beta + t_f f_b)\boldsymbol{K} + \boldsymbol{\sigma} + \boldsymbol{Z} + \boldsymbol{\chi} \\ &= \boldsymbol{\varphi_I} + 2\pi\lambda \cdot \boldsymbol{K} + \boldsymbol{\sigma} + \boldsymbol{Z} + \boldsymbol{\chi} \end{aligned} \tag{14}$$

For a specific frame, λ is a constant value and represents the sum of α, β, and $t_f f_b$. Besides, $\boldsymbol{\sigma}$ is also a constant for each subcarrier in the same frame and can be estimated by $\boldsymbol{\phi}$ [11]. Thus, we use $\boldsymbol{C}$ to replace the sum of $\boldsymbol{\sigma}$ and $\boldsymbol{Z}$. Then the received signal can be rewritten as:

$$\begin{aligned} \boldsymbol{\phi} &= \boldsymbol{\varphi_I} + 2\pi\lambda \cdot \boldsymbol{K} + \boldsymbol{C} + \boldsymbol{\chi} \\ &= 2\pi\lambda \cdot \boldsymbol{K} + (\boldsymbol{\varphi_I} + \boldsymbol{C}) + \boldsymbol{\chi} \\ &= 2\pi\lambda \cdot \boldsymbol{K} + \boldsymbol{C^*} + \boldsymbol{\chi} \end{aligned} \tag{15}$$

where $\boldsymbol{C^*}$ contains the real phase $\boldsymbol{\varphi_I}$ and the constant $\boldsymbol{C}$. According to [11], $\boldsymbol{C^*}$ can be estimated by the phases of a pair of mirror subcarriers measured at the receiver. Specifically, we sum the phases (ϕ_{-1} and ϕ_1) measured at the receiver of a pair of mirror subcarriers -1 and 1 (subcarriers 15 and 16 in CSITOOL) as the following equation:

$$\begin{aligned} \phi_{-1} + \phi_1 &= 2\pi\lambda \cdot (-1 + 1) + 2 \cdot \boldsymbol{C^*} + \chi_{-1} + \chi_1 \\ &= 2 \cdot \boldsymbol{C^*} + \chi_{-1} + \chi_1 \end{aligned} \tag{16}$$

where χ_{-1} and χ_1 are the NLPEs of subcarrier -1 and subcarrier 1 (subcarriers 15 and 16 in CSITOOL) respectively and $\chi_{-1} + \chi_1 \approx 0$ [18]. Thus, $\boldsymbol{C^*}$ can be calculated approximately as:

$$\boldsymbol{C^*} \approx \frac{\phi_{-1} + \phi_1}{2} \tag{17}$$

Here, $\boldsymbol{C^*}$ is subtracted from the phases of all received frames for the elimination of environmental impacts. After the elimination, the normalized phases across subcarriers, as shown in Fig. 6(a), are evenly distributed on both sides of the X-axis and approximately centrosymmetry with the center subcarrier.

Elimination of hardware impacts and Obtain NLPEV: After eliminating the environmental impacts, the total NLPE $\boldsymbol{\chi}$ caused by imperfect hardware design and human motion can be expressed as:

$$\boldsymbol{\chi} \approx \boldsymbol{\phi}_E - 2\pi\lambda \cdot \boldsymbol{K} \tag{18}$$

where $\boldsymbol{\phi}_E$ denotes the normalized phases after subtracting $\boldsymbol{C^*}$. To obtain a relatively steady NLPE $\boldsymbol{\chi}$ and to reduce the impact of location on motion waveforms, similar to [18], we use the deviation between the normalized phases $\boldsymbol{\phi}_E$ and the fitted line $\boldsymbol{L}$ to represent the stable NLPE $\boldsymbol{\chi_{st}}$. Especially, the fitted line $\boldsymbol{L}$ is generated by connecting two points, i.e., $(-28, \phi_{E,-28})$ and $(28, \phi_{E,28})$ (corresponding to subcarriers 1 and 30 in CSITOOL), which can be expressed as:

$$\begin{aligned} \boldsymbol{L} &= slope \cdot \boldsymbol{K} + bias \\ &= \frac{\phi_{E,28} - \phi_{E,-28}}{56} \cdot \boldsymbol{K} + \frac{\phi_{E,-28} + \phi_{E,28}}{2} \end{aligned} \tag{19}$$

Thus, the stable NLPE $\boldsymbol{\chi_{st}}$ can be obtained by:

$$\boldsymbol{\chi}_{st} = \boldsymbol{\phi}_E - \boldsymbol{L} \tag{20}$$

Since the NLPE caused by imperfect hardware design $\boldsymbol{\psi}$ is a constant for the specific network card [18] and $\boldsymbol{\eta}_{em}$ equals

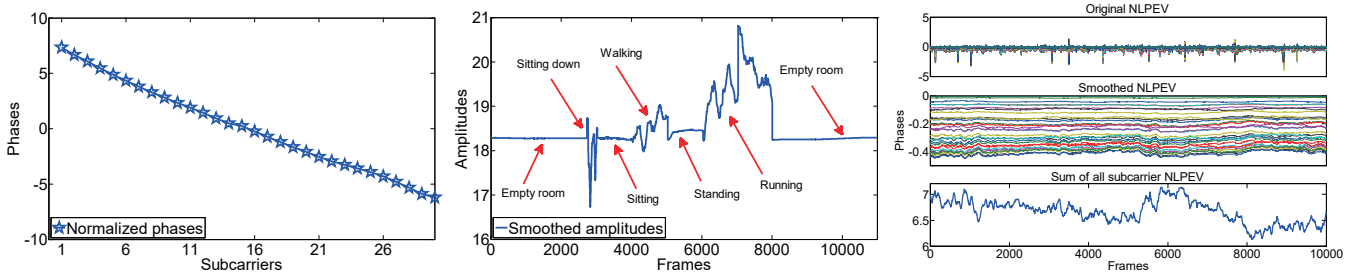

(a) Normalized phases after elimination of environmental impacts. **(b)** Segmentation based on CSI amplitudes. **(c)** NLPEV data smoothing for running frames.

Fig. 6 Phase and amplitude adaptive processing.

0 when there is no motion in the range, we can calculate ψ_{em} in an empty room without human motion:

$$\begin{aligned} \psi_{em} + \eta_{em} &= \phi_{E,em} - \boldsymbol{L}_{em} \\ \psi_{em} &= \phi_{E,em} - \boldsymbol{L}_{em} \end{aligned} \tag{21}$$

where $\phi_{E,em}$ and $\boldsymbol{L}_{em}$ denote the normalized phases and the fitted line in the empty room, respectively. Then, ψ_{em} is used to represent the NLPE caused by imperfect hardware design in all frames. Here, we subtract ψ_{em} from the stable NLPE χ_{st} of each received frame for the elimination of hardware impacts. Thus, the NLPEV η caused by human movement of each frame can be obtained by:

$$\begin{aligned} \eta &= \chi_{st} - \psi_{em} \\ &= \phi_E - \boldsymbol{L} - \psi_{em} \end{aligned} \tag{22}$$

Adaptive Segmentation and Filtering: To reduce the impact of background environment and obtain high energy-efficiency, the dynamic segmentation is employed in PhaseAnti. Since amplitude information has better continuity [21] and amplitude and phase are synchronized for the same frame, NLPEV is segmented according to the results of amplitude segmentation. To obtain stable CSI amplitudes and make them amenable for data segmentation, the high-frequency glitches need to be eliminated. Specifically, we leverage *Hampel Filter* [23], which is proved to be useful for wireless signals [9] to reduce high-frequency amplitude glitches using a sliding window of 500 frames and the threshold of 0.01. Fig. 6(b) depicts the amplitudes after filtering. The smoothed amplitude is a straight line with small fluctuations when there is no one in the range, and the variation becomes significant when the person is moving. Thus, an effective algorithm [24] based on the amplitude gradient threshold is used for motion sample segmentation.

Then, the adaptive *Hampel Filter* is used for NLPEV glitch elimination with the same sliding window size as the amplitude segmentation and the threshold of 0.01. Fig. 6(c) presents the NLPEV calibration results. The original NLPEV of all subcarriers has high-frequency noises. However, after implementing the proposed adaptive smoothing scheme, the high-frequency noises are removed. Moreover, the sum of the absolute values of each subcarrier NLPEV clearly shows that the same motion has similar NLPEV waveforms.

Subcarrier Selection: To further boost the reliability of NLPEV data and to reduce computation complexity, a

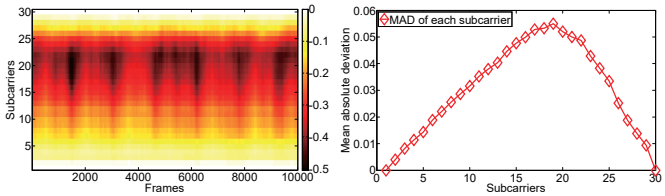

(a) NLPEV series patterns for running frames. **(b)** Mean absolute deviation of each subcarrier.

Fig. 7 Subcarrier selection.

subcarrier selection algorithm is employed in PhaseAnti. Since different subcarriers have distinct wavelengths, the sensitivity of subcarriers for motions is also different. Generally, the larger mean absolute deviation (MAD) caused by movement represents the higher sensitivity of the subcarrier. Thus, the MAD of NLPEV data for all subcarriers is used to measure its sensitivity. Specifically, for the given training and testing sets, we first choose u maximum MADs of NLPEV data from all motion frames. Then, to better satisfy all subcarrier spatial characteristics and enhance the data stability, the median of u MADs of NLPEV data is used as the final selection. Fig. 7(a) shows the NLPEV series patterns for the running frames, and we can observe that the neighboring subcarriers of subcarrier 20 have a higher sensitivity to the running frames. Besides, Fig. 7(b) depicts the MAD of each subcarrier for all motion frames, and the NLPEV MAD of the 19^{th} subcarrier is the maximum. In PhaseAnti, we set the $u = 3$ as the default value, and subcarriers 19,18 and 17 are thus selected. With the above approach, subcarrier 18 is finally chosen.

B. Feature Extraction and Classification

To perform a fair comparison, for both amplitude and NLPEV data, we extract the same 10 statistic features from both time and frequency domains, which are widely used in the WiFi-based HAR systems [6]–[8], [10]. Specifically, the time-domain features are mean, variance, maximum, minimum, median, first quartile, and third quartile. The frequency-domain features are information entropy, spectrum energy, and maximum frequency domain. To evaluate the performance under different classifiers, five classical classification approaches are used to recognize activities, which are the Random Forest (RF), the Decision Tree (DT), the k-NearestNeighbor (kNN), the Logistic Regression (LR) and the Support Vector Machine (SVM).

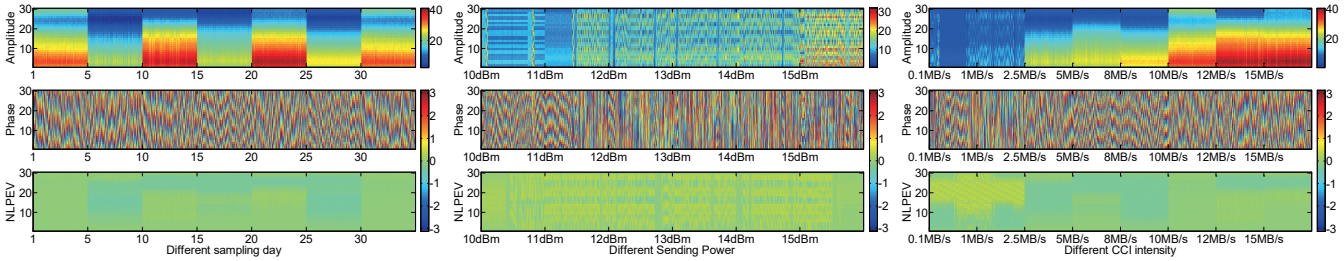

(a) NLPEV remains invariant across the time. **(b)** NLPEV remains invariant under the different sending power. **(c)** NLPEV remains invariant under the different interference traffic rates.

Fig. 8 Observation of invariance of amplitude, phase, and NLPEV with respect to time, sending power, and CCI intensity.

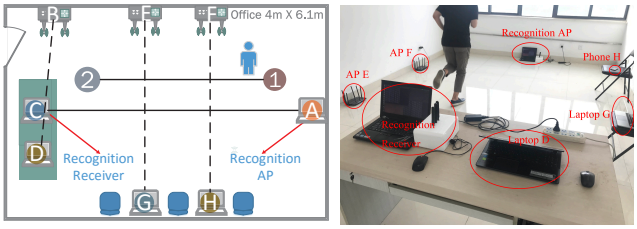

(a) The schematic diagram. **(b)** Experimental setting.

Fig. 9 Evaluation scenario in a conference room.

IV. Implementation And Evaluation

A. Implementation

In the experiments, we use two Lenovo laptops as a recognition access point (RAP) and a recognition receiver (RR), respectively, both equipped with the Intel 5300 NIC with three antennas. Besides, we use three TP-link WiFi routers as interference APs (IAPs) and three other devices (mobile phone or laptops) as interference receiver (IR). PhaseAnti is implemented on the Ubuntu desktop 14.04 LTS OS for both RAP and RR. PhaseAnti uses the laptop RR to collect per frame CSI at a rate of 100 frames per second using CSITOOL [17].

Deployment: We conducted extensive experiments with 8 persons over one month. As shown in Fig. 9, the $6.1 \times 4m^2$ test scenarios include a computer table and several chairs. The distance between point 1 and point 2 is $3m$. Besides, four different actions, i.e., standing at point 1, walking between point 1 and point 2, running between point 1 and point 2 and sitting at point 1, and a reference state, i.e., the empty room, are design to observe the impact of CCI on CSI signals with or without human movement.

A comparison experiment is given to measure the impact of various CCI on CSI, including the following scenarios:

- **Non-interfering scenario:** RAP A is set to channel 1 and forms a wireless link with RR C. AP B, laptop D, and other devices are powered off.
- **Simple and constant CCI scenario:** Based on the above setting, AP B is powered on and set to channel 3 since half of channel 3 subcarriers are overlapped with the subcarriers of channel 1. Then, Laptop D is powered on and connected to AP B with 2.5 MB/s ITR (100 frames/s with 25000 bytes packet length).
- **Complex and varying CCI scenario:** In addition to the above settings, mobile phone G and laptop H are powered on and connected to APs E and F, respectively. The ITR of mobile phone G and laptop H are 1 MB/s and 5 MB/s, respectively. Moreover, APs B, E, and F are adjusted from channel 1 to channel 5 to produce a varying CCI since only channel 1 to 5 overlap with the RAP A channel.

We examine the performance of single-user motion recognition in three given scenarios. For every participant of 8 people in each CCI scenario, we collect 54 samples of each motion or state. Thus, a total of $3 \times 8 \times 5 \times 54$ (6480) activity samples are collected for training and testing.

B. CCI Robustness Assessment of NLPEV

Invariant to CCI and stable across time are essential attributes for a CCI robustness signal component. However, under different CCI scenarios, APs change the sending power to better compete for the channel [12]. Besides, the sampling rate also decreases as the increase of CCI ITR [25]. Thus, we demonstrate the invariance of NLPEV to time, sending power, and CCI ITR by experiments.

Time Invariance: For HAR systems, the signal component used for recognition should be invariant at different sampling time. However, it is non-negligible that CSIs may change due to different temperatures and humidity of different days [18]. Since NLPEV is also a phase component extracted from CSI, it is vital to ensure the stability of NLPEV across time. Fig. 8(a) shows amplitude, phase, and NLPEV at different time without human motion. We measure the CSI in the conference room, as shown in Fig. 9, and extracted NLPEVs, day and night for a month. We can see that amplitude change with different sampling days and phase change randomly due to phase errors. However, NLPEVs are relative stability and invariant across time.

Sending Power Invariance: In order to examine the invariance of NLPEV to the change of sending power caused by AP competing for the channel, as shown in Fig. 9(a), we change the NIC power of RR C from 10 dBm to 15 dBm (maximum power of 5300 NIC) and fix the power of RAP A. Then, the sampled CSIs and the extracted NLPEVs in different sending power are shown in Fig. 8(b). It is evident that amplitude increases with the rising sending power. However, NLPEV changes negligibly with the increasing sending power, which clearly demonstrates that NLPEV is more stable and independent of the varying signal strength.

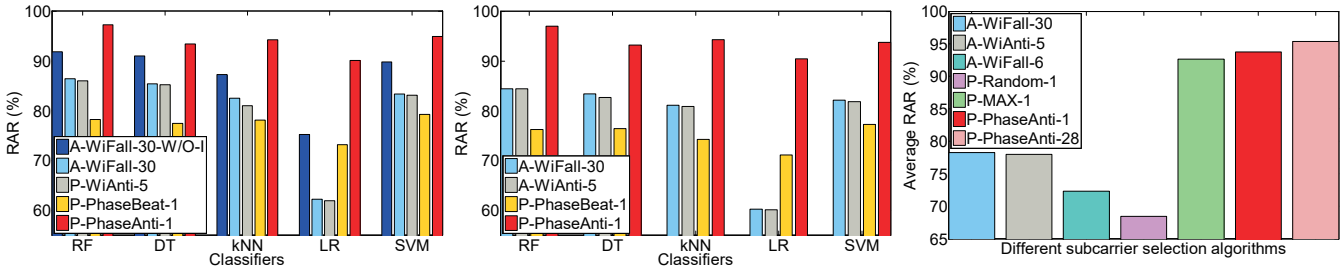

(a) Comparison of different system RARs in the simple CCI scenario under various classifiers. **(b)** Comparison of different system RARs in the complex CCI scenario under various classifiers. **(c)** Average RARs of different subcarrier selection algorithms in the complex CCI scenario.

Fig. 10 Comparison of the different algorithm performance. A: use amplitude information, P: use phase information. Middle word: the corresponding algorithm and used signal component. Last number: the number of used subcarriers.

CCI Intensity Invariance: The increase of CCI intensity causes a decrease in the sampling rate and the confusion of the receiving packet order [15]. Thus, the stability of CSI is affected. To evaluate the impact of this factor on NLPEV, we keep one IAP (router B in Fig. 9(a)) and adjust ping rates and packet lengths of the interferer, as shown in Fig. 8(c), to set different ITRs. Fig. 8 depicts that amplitude increases significantly due to the increasing of sending power caused by AP competing for the channel in more severe CCI scenarios. However, NLPEV stays almost constant even if the CCI ITR is changing. This experiment confirms that NLPEV is invariant to various CCI intensities.

C. Performance of Activity Recognition

Accuracy: The recognition accuracy rate (RAR) used in this paper is defined as the ratio of the number of correctly classified activities to the number of the whole testing activities. 10-fold cross-validation [26] is used to avoid overfitting. Besides, we compare the proposed method using a single subcarrier (P-PhaseAnti-1) with the pioneer amplitude-based method [7] using 30 subcarriers (A-WiFall-30), the state-of-the-art anti-CCI algorithm [15] using 5 subcarriers (A-WiAnti-5), and the pioneer phase-based method [9] using a single subcarrier (P-PhaseBeat-1).

Fig. 10(a) shows the RARs of different algorithms in the simple CCI scenario, as introduced in Section IV-A. As a reference state in the non-interfering environment, A-WiFall-30-W/O-I denotes the RAR of WiFall using 30 subcarriers in the scenario without CCI. The rest of the experimental results of Fig. 10(a) are obtained in the simple CCI scenario. As shown in Fig. 10(a), although only one subcarrier is used, P-PhaseAnti-1 can still achieve better performance compared with the baselines in all cases. Since all subcarriers are used in A-WiFall-30, the RAR of this method represents the upper limit of the amplitude method. However, the computational complexity of A-WiFll-30 is too big for real-time HAR. Compared with WiFall, the pioneer anti-CCI algorithm WiAnti only uses 5 subcarriers and obtains similar RARs close to A-WiFall-30 due to the consideration of subcarrier correlation. However, since amplitude inevitably changes with varying CCI, the performance of A-WiAnti-5 is limited. Compared with WiAnti, P-PhaseAnti-1 can achieve better performance since the phase component NLPEV used for recognition is independent of CCI. Specifically, among five different classifiers testing, P-PhaseAnti-1 achieves 93.98% RAR on average, which is 14.53% higher than the pioneer anti-CCI method A-WiAnti-5. Besides, for the non-interfering environment, the performance of A-WiFall-30-W/O-I has a significant improvement compared with the same method in CCI scenarios. This means that the state-of-the-art methods are indeed affected by CCI. However, P-PhaseBeat-1 gets 6.97% higher RAR than A-WiFall-30-W/O-I on average. This means that the NLPEV used by PhaseAnti contains more motion information than the amplitude, even without the effects of CCI.

Fig. 10(b) shows the experimental results in the complex CCI scenario. Compared with the simple CCI scenario, the RARs of all baseline methods decrease due to the more severe CCI. Nevertheless, P-PhaseAnti-1 keeps almost the same and consistently outperform A-WiFall-30, A-WiAnti-5, and P-PhaseBeat-1 in terms of RAR. Since the complex CCI environment for each algorithm is consistent, higher RAR means less impact of CCI to the signal component and better ability to maintain motion information.

We further test the performance of various data dimension reduction algorithms under the complex CCI, and the results are shown in Fig. 10(c). Especially, the average RAR represents the average performance of five different classifiers. A-WiFall-6 denotes the useful subcarrier fusion algorithm, as introduced in [7]. P-MAX-1 means selecting the subcarrier with the maximum NLPEV MAD for all motion frames (e.g., subcarrier 19 in Fig. 7(b)), and P-Random-1 denotes randomly selecting one subcarrier NLPEV data. Besides, P-PhaseAnti-28 represents using all subcarrier NLPEV data to perform HAR (except subcarriers 1 and 30 in CSITOOL). Due to the consideration of subcarrier spatial characteristics and the stability of data, P-PhaseAnti-1 outperforms P-MAX-1 and P-Random-1 in terms of average RAR. This means the choice of median makes the data more robust. Moreover, the RAR of P-PhaseAnti-1 is close to the RAR of P-PhaseAnti-28. This means that although only one subcarrier is used, most motion information can be maintained by our valid subcarrier selection algorithm.

Classification: Two confusion matrices that using RF as a classifier are illustrated to demonstrate the robustness of algorithms to similar motions (running and walking) in the

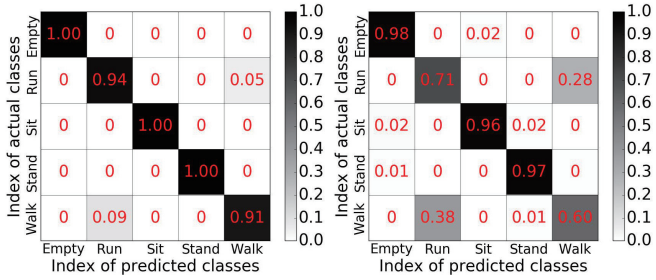

(a) P-PhaseAnti-1 uses RF in the complex CCI scenario.

(b) A-WiFall-30 uses RF in the complex CCI scenario.

Fig. 11 Confusion matrices for different systems.

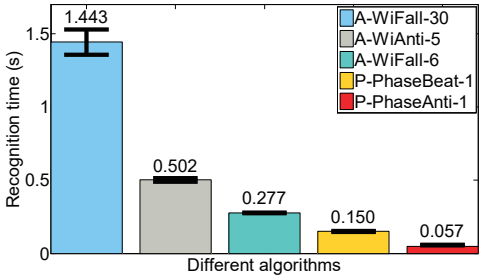

Fig. 12 Comparison of various algorithm recognition time.

complex CCI scenario. From Fig. 11(a), we can observe that P-PhaseAnti-1 can not only classify normal actions, i.e., empty room, sitting, and standing, with high RARs close to 100% but also achieves 93% RAR of the similar activities, i.e., walking and running in the complex CCI scenario. In contrast, Fig. 11(b) depicts that the amplitude-based method A-WiFall-30 achieves high RARs on normal motions. However, complex CCI has considerable side effects on similar activity RARs. Thus, PhaseAnti is more robust for similar motion classification in the complex CCI scenario.

Speed: Fig. 12 shows the recognition time of a single motion sample for different algorithms, including the time of signal processing and the time of classification. Compared with the method using all subcarriers (A-WiFall-30), the pioneer anti-CCI method WiAnti can realize 3× faster recognition speed due to the valid subcarrier selection. However, since only one subcarrier is used, P-PhaseAnti-1 can recognize the activity with minimal time (0.057s) and nearly 9× faster than the pioneer anti-CCI solution WiAnti.

V. Related Work

Wireless sensing HAR systems can be broadly classified into three categories:

Specialized hardware-based: Fine-grained radio frequency signals can be collected by the specially designed hardware [24], [27], [28]. WiSee [27] used USRP to capture the Doppler shift in body reflected signals to recognize a set of nine gestures with high accuracy. TagFree [28] used the Thingmagic reader to collect the multipath signals from different RFID tags to classify the working motions. However, the specialized equipment used by these methods is irreplaceable but expensive.

RSSI-based: RSSI is an indication to measure the power of the received radio signals. Since different activities cause distinct RSSI fluctuations, activities can be recognized accordingly by signal processing. PAWS [29] explored WiFi ambient signals for establishing RSSI fingerprint of different activities. Wigest [30] leveraged changes in WiFi RSSI to sense in-air hand gestures around the mobile device. However, these methods can only do coarse-grained HAR since RSSI falls entirely in the time domain, while the frequency domain is totally neglected. Besides, suffering from performance degradation due to the multipath effect is also a problem for RSSI-based systems [31].

CSI-based: In contrast, CSI is a fine-grained value derived from the physical layer of the off-the-shelf WiFi device. Features are descriptions of motion from different perspectives, i.e., time domain and frequency domain. Thus, compared with RSSI, more information can be obtained from CSIs. Many excellent solutions have been proposed. PhaseBeat [9] exploited CSI phase difference data to monitor breathing and heartbeats. WiKey [8] recognized the typed keys based on CSI values to collect password information. PERFIC [14] amended the abnormal WiFi subcarriers to recognize motions in cross-technology interference (caused by Bluetooth or Zigbee) scenarios. However, most existing works based on WiFi do not consider the impact of CCI caused by other WiFi devices, and their experimental results are based on a non-CCI environment. Furthermore, the performance of these systems degrades due to CCI. Although WiAnti [15] proposed a subcarrier selection algorithm to select most information subcarriers to realize anti-interference, this algorithm still stays at the signal processing level and does not propose the CCI-independent CSI component. Moreover, the varying CSI amplitude limits its performance.

In summary, inspired by the prior works, the contributions of our work lie in obtaining CCI-independence CSI phase component NLPEV, which is different for distinct activities and using this component to perform HAR with high RAR and low recognition time in CCI scenarios. To the best of our knowledge, it is the first to leverage the interference-independence CSI component from a commodity WiFi device to recognize activities accurately in CCI scenarios.

VI. Conclusion

In this paper, we propose PhaseAnti, an anti-CCI HAR system based on WiFi CSI. Specifically, by eliminating irrelevant errors, the interference-independent phase component NLPEV is leveraged from the off-the-shelf WiFi device since this component keeps invariant for CCI and contains motion information. Then, a suitable calibration method is introduced to make NLPEV data stable and sensitive to motions. Next, to reduce the data dimension, a novel subcarrier selection algorithm is used with less information loss. Finally, by using this calibrated NLPEV data of the selected subcarrier to perform HAR in CCI scenarios, the activity can be recognized accurately with low recognition time. Extensive experiments with different motions are implemented in various CCI scenarios, and the results show that PhaseAnti can achieve superior performance on RAR and recognition time over existing methods in all cases.

REFERENCES

[1] Oscar D Lara and Miguel A Labrador, "A survey on human activity recognition using wearable sensors.," *IEEE Communications Surveys and Tutorials*, vol. 15, no. 3, pp. 1192–1209, 2013.

[2] Amir Shahroudy, Tian-Tsong Ng, Qingxiong Yang, and Gang Wang, "Multimodal multipart learning for action recognition in depth videos," *IEEE transactions on pattern analysis and machine intelligence*, vol. 38, no. 10, pp. 2123–2129, 2016.

[3] Mostafa S Ibrahim, Srikanth Muralidharan, Zhiwei Deng, Arash Vahdat, and Greg Mori, "A hierarchical deep temporal model for group activity recognition," in *Proceedings of the IEEE Conference on Computer Vision and Pattern Recognition*, 2016, pp. 1971–1980.

[4] Jess McIntosh, Charlie McNeill, Mike Fraser, Frederic Kerber, Markus Löchtefeld, and Antonio Krüger, "Empress: Practical hand gesture classification with wrist-mounted emg and pressure sensing," in *Proceedings of the 2016 CHI Conference on Human Factors in Computing Systems*. ACM, 2016, pp. 2332–2342.

[5] Wenchao Jiang and Zhaozheng Yin, "Human activity recognition using wearable sensors by deep convolutional neural networks," in *Proceedings of the 23rd ACM international conference on Multimedia*. Acm, 2015, pp. 1307–1310.

[6] Yan Wang, Jian Liu, Yingying Chen, Marco Gruteser, Jie Yang, and Hongbo Liu, "E-eyes: device-free location-oriented activity identification using fine-grained wifi signatures," in *Proceedings of the 20th annual international conference on Mobile computing and networking*. ACM, 2014, pp. 617–628.

[7] Yuxi Wang, Kaishun Wu, and Lionel M Ni, "Wifall: Device-free fall detection by wireless networks," *IEEE Transactions on Mobile Computing*, vol. 16, no. 2, pp. 581–594, 2017.

[8] Kamran Ali, Alex X Liu, Wei Wang, and Muhammad Shahzad, "Recognizing keystrokes using wifi devices," *IEEE Journal on Selected Areas in Communications*, vol. 35, no. 5, pp. 1175–1190, 2017.

[9] Xuyu Wang, Chao Yang, and Shiwen Mao, "Phasebeat: Exploiting csi phase data for vital sign monitoring with commodity wifi devices," in *Distributed Computing Systems (ICDCS), 2017 IEEE 37th International Conference on*. IEEE, 2017, pp. 1230–1239.

[10] Kun Qian, Chenshu Wu, Zimu Zhou, Yue Zheng, Zheng Yang, and Yunhao Liu, "Inferring motion direction using commodity wi-fi for interactive exergames," in *Proceedings of the 2017 CHI Conference on Human Factors in Computing Systems*. ACM, 2017, pp. 1961–1972.

[11] Nan Yu, Wei Wang, Alex X Liu, and Lingtao Kong, "Qgesture: Quantifying gesture distance and direction with wifi signals," *Proceedings of the ACM on Interactive, Mobile, Wearable and Ubiquitous Technologies*, vol. 2, no. 1, pp. 51, 2018.

[12] "Ieee standard for information technology," *IEEE Std 802.11n-2009*, pp. 1–565, Oct 2009.

[13] Feng Li, Jun Luo, Gaotao Shi, and Ying He, "Art: Adaptive frequency-temporal co-existing of zigbee and wifi," *IEEE Transactions on Mobile Computing*, vol. 16, no. 3, pp. 662–674, 2017.

[14] Yue Zheng, Zheng Yang, Junjie Yin, Chenshu Wu, Kun Qian, Fu Xiao, and Yunhao Liu, "Combating cross-technology interference for robust wireless sensing with cots wifi," in *2018 27th International Conference on Computer Communication and Networks (ICCCN)*. IEEE, 2018, pp. 1–9.

[15] Jinyang Huang, Bin Liu, Hongxin Jin, and Zhiqiang Liu, "Wianti: an anti-interference activity recognition system based on wifi csi," in *2018 IEEE International Conference on Internet of Things (iThings) and IEEE Green Computing and Communications (GreenCom) and IEEE Cyber, Physical and Social Computing (CPSCom) and IEEE Smart Data (SmartData)*. IEEE, 2018, pp. 58–65.

[16] Xuyu Wang, Lingjun Gao, Shiwen Mao, and Santosh Pandey, "Csi-based fingerprinting for indoor localization: A deep learning approach," *IEEE Transactions on Vehicular Technology*, vol. 66, no. 1, pp. 763–776, 2017.

[17] Daniel Halperin, Wenjun Hu, Anmol Sheth, and David Wetherall, "Tool release: Gathering 802.11 n traces with channel state information," *ACM SIGCOMM Computer Communication Review*, vol. 41, no. 1, pp. 53–53, 2011.

[18] Pengfei Liu, Panlong Yang, Wen-Zhan Song, Yubo Yan, and Xiang-Yang Li, "Real-time identification of rogue wifi connections using environment-independent physical features," in *Proceedings of IEEE INFOCOM 2019-IEEE Conference on Computer Communications*, 2019.

[19] Youwei Zeng, Dan Wu, Ruiyang Gao, Tao Gu, and Daqing Zhang, "Fullbreathe: Full human respiration detection exploiting complementarity of csi phase and amplitude of wifi signals," *Proceedings of the ACM on Interactive, Mobile, Wearable and Ubiquitous Technologies*, vol. 2, no. 3, pp. 148, 2018.

[20] Yiwei Zhuo, Hongzi Zhu, Hua Xue, and Shan Chang, "Perceiving accurate csi phases with commodity wifi devices," in *INFOCOM 2017-IEEE Conference on Computer Communications, IEEE*. IEEE, 2017, pp. 1–9.

[21] Wei Wang, Alex X Liu, Muhammad Shahzad, Kang Ling, and Sanglu Lu, "Understanding and modeling of wifi signal based human activity recognition," in *Proceedings of the 21st Annual International Conference on Mobile Computing and Networking*. ACM, 2015, pp. 65–76.

[22] J Stuart Hunter, "The exponentially weighted moving average," *Journal of quality technology*, vol. 18, no. 4, pp. 203–210, 1986.

[23] Ronald K Pearson, "Outliers in process modeling and identification," *IEEE Transactions on control systems technology*, vol. 10, no. 1, pp. 55–63, 2002.

[24] Ning Xiao, Panlong Yang, Yubo Yan, Hao Zhou, and Xiang-Yang Li, "Motion-fi: Recognizing and counting repetitive motions with passive wireless backscattering," in *IEEE INFOCOM 2018-IEEE Conference on Computer Communications*. IEEE, 2018, pp. 2024–2032.

[25] Souvik Sen, Romit Roy Choudhury, and Srihari Nelakuditi, "Csma/cn: Carrier sense multiple access with collision notification," *IEEE/ACM Transactions on Networking (ToN)*, vol. 20, no. 2, pp. 544–556, 2012.

[26] Ron Kohavi et al., "A study of cross-validation and bootstrap for accuracy estimation and model selection," in *Ijcai*. Montreal, Canada, 1995, vol. 14, pp. 1137–1145.

[27] Qifan Pu, Sidhant Gupta, Shyamnath Gollakota, and Shwetak Patel, "Whole-home gesture recognition using wireless signals," in *Proceedings of the 19th annual international conference on Mobile computing & networking*. ACM, 2013, pp. 27–38.

[28] Xiaoyi Fan, Wei Gong, and Jiangchuan Liu, "Tagfree activity identification with rfids," *Proceedings of the ACM on Interactive, Mobile, Wearable and Ubiquitous Technologies*, vol. 2, no. 1, pp. 7, 2018.

[29] Yu Gu, Fuji Ren, and Jie Li, "Paws: Passive human activity recognition based on wifi ambient signals," *IEEE Internet of Things Journal*, vol. 3, no. 5, pp. 796–805, 2016.

[30] Heba Abdelnasser, Moustafa Youssef, and Khaled A Harras, "Wigest: A ubiquitous wifi-based gesture recognition system," in *Computer Communications (INFOCOM), 2015 IEEE Conference on*. IEEE, 2015, pp. 1472–1480.

[31] Bryce Kellogg, Vamsi Talla, and Shyamnath Gollakota, "Bringing gesture recognition to all devices," in *11th {USENIX} Symposium on Networked Systems Design and Implementation ({NSDI} 14)*, 2014, pp. 303–316.